





Robust Reconstruction of Historical Climate Change From Permafrost Boreholes


Special Collection:

The Arctic: An AGU Joint Special Collection

Brian Groenke^{1,2} , Moritz Langer^{1,3}, Frederieke Miesner^{1,4} , Sebastian Westermann⁴ , Guillermo Gallego^{2,5}, and Julia Boike^{1,6} 

¹Permafrost Research Section, Alfred Wegener Institute Helmholtz Center for Polar and Marine Research, Potsdam, Germany, ²Department of Electrical Engineering and Computer Science, Technical University of Berlin, Berlin, Germany, ³Department of Earth Sciences, Vrije Universiteit Amsterdam, Amsterdam, The Netherlands, ⁴Department of Geosciences, University of Oslo, Oslo, Norway, ⁵Einstein Center Digital Future and Science of Intelligence Excellence Cluster, Berlin, Germany, ⁶Department of Geography, Humboldt University, Berlin, Germany

Key Points:

- We propose a new method to estimate historical ground surface temperatures from boreholes in permafrost using Bayesian inverse modeling
- We evaluate our method on both synthetic test cases for cold and warm conditions as well as real data from a 100 m deep borehole in Siberia
- We find that seasonal freezing and thawing of the active layer has a significant impact on the reconstructed ground surface temperatures

Correspondence to:

 B. Groenke,
brian.groenke@awi.de
Citation:

Groenke, B., Langer, M., Miesner, F., Westermann, S., Gallego, G., & Boike, J. (2024). Robust reconstruction of historical climate change from permafrost boreholes. *Journal of Geophysical Research: Earth Surface*, 129, e2024JF007734. <https://doi.org/10.1029/2024JF007734>

Received 12 MAR 2024

Accepted 17 JUN 2024

Author Contributions:
Conceptualization: Brian Groenke, Moritz Langer

Data curation: Frederieke Miesner, Julia Boike

Formal analysis: Brian Groenke

Funding acquisition: Guillermo Gallego, Julia Boike

Investigation: Brian Groenke, Moritz Langer, Frederieke Miesner, Sebastian Westermann

Methodology: Brian Groenke, Frederieke Miesner, Sebastian Westermann

Project administration: Brian Groenke, Guillermo Gallego, Julia Boike

Software: Brian Groenke

© 2024 The Authors.

This is an open access article under the terms of the [Creative Commons Attribution-NonCommercial License](https://creativecommons.org/licenses/by-nc/4.0/), which permits use, distribution and reproduction in any medium, provided the original work is properly cited and is not used for commercial purposes.

Abstract Reconstructing historical climate change from deep ground temperature measurements in cold regions is often complicated by the presence of permafrost. Existing methods are typically unable to account for latent heat effects due to the freezing and thawing of the active layer. In this work, we propose a novel method for reconstructing historical ground surface temperature (GST) from borehole temperature measurements that accounts for seasonal thawing and refreezing of the active layer. Our method couples a recently developed fast numerical modeling scheme for two-phase heat transport in permafrost soils with an ensemble-based method for approximate Bayesian inference. We evaluate our method on two synthetic test cases covering both cold and warm permafrost conditions as well as using real data from a 100 m deep borehole on Sardakh Island in northeastern Siberia. Our analysis of the Sardakh Island borehole data confirms previous findings⁴ that GST in the region have likely risen by 5–9°C between the pre-industrial period of 1750–1855 and 2012. We also show that latent heat effects due to seasonal freeze-thaw have a substantial impact on the resulting reconstructed surface temperatures. We find that neglecting the thermal dynamics of the active layer can result in biases of roughly -1°C in cold conditions (i.e., mean annual ground temperature below -5°C) and as much as -2.6°C in warmer conditions where substantial active layer thickening (>200 cm) has occurred. Our results highlight the importance of considering seasonal freeze-thaw in GST reconstructions from permafrost boreholes.

Plain Language Summary Long-term changes in the temperature of the atmosphere are recorded in the solid Earth due to the insulating properties of soil and rock. As a result, it is possible to estimate past changes in temperature at the interface between the ground and the atmosphere by measuring ground temperatures deep below Earth's surface. In cold regions, the presence of permafrost, that is, ground that remains frozen throughout the year, complicates such analyses due to the effects of water freezing and thawing in the soil. In this work, we present a new method for reconstructing past changes in ground surface temperature from boreholes situated in permafrost using a computational model of heat flow that accounts for these effects. We evaluate our method on both synthetic test cases as well as real data from a 100 m deep borehole in northeastern Siberia. Our results demonstrate that annual freezing and thawing of water near the surface has a substantial impact on the reconstructed ground surface temperature (GST), especially in regions where permafrost is thawing. The proposed method is the first to be widely applicable to ground temperatures measured in permafrost and thus constitutes a valuable new tool for understanding past and present climate change in cold regions.

1. Introduction

Reconstructing historical climate change is crucial to provide context for the recent warming trends observed in the late 20th and early 21st centuries. Global instrumental surface-air temperature records date back only to the mid-19th century (Benestad et al., 2019), and such long-term records are even more limited in Arctic regions (Gilichinsky et al., 1998) where much of the surface is underlain by permafrost, that is, ground that remains perennially frozen. Recent studies have established from ground temperature records that permafrost is warming globally over the last two decades (Biskaborn et al., 2019). Long-term historical simulations of land surface heat exchange (Langer et al., 2024) as well as ice core reconstructions (Opel et al., 2013) suggest that this warming trend likely dates back to the conclusion of the Little Ice Age in the early to mid-19th century. However,

Supervision: Moritz Langer, Guillermo Gallego, Julia Boike
Validation: Brian Groenke
Writing – original draft: Brian Groenke
Writing – review & editing: Brian Groenke, Moritz Langer, Frederieke Miesner, Sebastian Westermann, Guillermo Gallego, Julia Boike

paleoclimate reconstructions from proxy data carry with them significant uncertainties (Hernández et al., 2020) and thus may not always be representative for terrestrial permafrost regions.

Temperature measurements from deep boreholes provide a valuable source of insight into how the thermal state of the Earth has evolved over time scales ranging from decades to millennia. This is possible due to the fact that temperature fluctuations at the surface diffuse relatively slowly through rock and soil (Huang et al., 2000). The solid Earth thereby acts as a low-pass filter that smooths the temperature signal over long time frames, with the length-scale of the smoothing kernel increasing with depth. As a result, it is possible to detect past changes in ground surface temperature (GST) from deep borehole temperature measurements (Lachenbruch & Marshall, 1986). Since its original conception by Beck and Judge (1969), this problem has been extensively studied (Dahl-Jensen et al., 1998; Huang et al., 1996; Mann et al., 2003; Pollack et al., 1998; Shen & Beck, 1991; Vasseur et al., 1983). One of the most commonly applied solutions uses singular value decomposition to solve the linear inverse problem posed by an analytical forward model of heat transport (Mareschal & Beltrami, 1992). This approach was recently augmented by Cuesta-Valero et al. (2022) to account for uncertainty through a bootstrap sampling approach. Such methods are, however, limited to simple forward models of conductive heat transport to which linear inversions are applicable. Furthermore, they do not easily permit the inclusion of a priori information about surface temperatures or other unknowns. Since the problem of inverse heat flow is fundamentally ill-posed (Alifanov, 2012), that is, there are an infinite number of solutions given any particular observed temperature profile, a priori constraints are often vital in identifying the most likely solutions given all available information. Bayesian approaches to GST reconstruction have the advantage of allowing for the direct incorporation of such information through prior distributions while also fully accounting for uncertainty in the inferred GST histories (Wang, 1992; Woodbury & Ferguson, 2006). Hopcroft and Gallagher (2023) recently applied one such method (Hopcroft et al., 2007) to the International Heat Flow Commission database (Huang & Pollack, 1998) of 1,012 temperature profiles, reaffirming that 20th century warming is anomalous in comparison to the 500-year period prior to industrialization. This database, however, features relatively few profiles in Arctic and subarctic regions which are known to be warming 2–3 times faster than the global average (Isaksen et al., 2022).

Permafrost is often a key feature of the landscape in these cold regions. In areas underlain by permafrost, effective thermal diffusivity in the so-called “active layer”, that is, the top layer of ground subjected to annual freezing and thawing (Harris et al., 1988), can drop to $0.1 \text{ m}^2\text{yr}^{-1}$ ($3.17 \times 10^{-9} \text{ m}^2\text{s}^{-1}$) or lower during the thawing and refreezing seasons due to the effects of latent heat (D. Riseborough, 1990). This has two important implications for geothermal reconstructions of GST where permafrost exists: first, when surface temperatures are reconstructed as annual or multi-annual averages, that is, neglecting seasonal freezing and thawing, the reconstructed upper boundary represents the long-term average temperature at the top of the permafrost (TTOP) rather than that of the land surface (Lachenbruch & Marshall, 1986). Consequently, such reconstructions necessarily assume that the depth of the permafrost table does not change over the full reconstruction period since the spatial domain of the model is typically treated as constant. Second, in regions with warmer permafrost, here defined as those with mean annual ground temperatures (MAGT) $\geq -5^\circ\text{C}$ (Nitzbon et al., 2023), and finer grained soils with moderate to high silt or clay content, latent heat effects may be present even well below the top of the permafrost (Nicolosky & Romanovsky, 2018; Romanovsky & Osterkamp, 2000). This is due to the persistence of unfrozen water in soil pores at subzero temperatures as a result of capillary action (Koopmans & Miller, 1966). The presence of such effects generally precludes the application of most existing GST reconstruction techniques, which typically ignore non-conductive heat transport, to borehole temperature measurements in permafrost soils (Beltrami, 1996; Mann & Schmidt, 2003; Mottaghy & Rath, 2006). As a result, most studies which have applied such methods to boreholes in cold regions have either neglected seasonal freezing and thawing (Kneier et al., 2018), selected boreholes in low porosity material such as bedrock (Guglielmin et al., 2018; Isaksen et al., 2000), or omitted permafrost boreholes altogether from the analysis (Pollack et al., 2003). There is, therefore, a general need for GST reconstruction methods that can account for latent heat effects in frozen ground.

In this work, we propose a new method for inverting GST histories from permafrost boreholes where latent heat effects play a dominant role due to both seasonal and long-term thawing of ground ice. Our method builds upon the thermal modeling scheme of *CryoGridLite* (Langer et al., 2024), which allows for efficient, high-fidelity simulation of two-phase heat conduction over large time scales. Similar to Hopcroft et al. (2007), we employ a Bayesian formulation of the inverse problem that provides a probabilistic interpretation of uncertainty in the reconstructed GST histories and permits the inclusion of prior information where available. We adapt the Bayesian inverse modeling workflow of Groenke et al. (2023) to GST reconstruction in order to efficiently obtain

an approximate posterior distribution over plausible GST histories. We first evaluate the method on synthetic data sets where the “true” surface temperature history is known and compare GST parameterizations with and without latent heat effects included. We then further apply our method to a real-world temperature profile from a 100 m deep borehole on Sardakh Island in northeastern Siberia and reconstruct historical ground surface temperatures over the time period of 1750–2012.

2. Methods

2.1. Forward Model of Two-Phase Heat Transport

In order to recover past changes in GST from measured temperature profiles, a forward model of subsurface heat transport is required to map changes in temperature at the surface to the resulting ground temperature profiles. Vertical conductive heat transport in the Earth's subsurface can be represented according to the standard form of the heat equation, with the upper boundary set according to surface temperature and the lower boundary set to an appropriate geothermal heat flux (Jaeger, 1965; Lachenbruch & Marshall, 1986). The resulting temperature field can then be represented as deviations from the quasi-linear steady state solution:

$$T(z, t) = T_0 + \frac{Q_{\text{geo}}}{k(z)}z + \Delta T(z, t) \quad (1)$$

where $T = T(z, t)$ is the temperature field (K) over depth z (m) and time t (s), T_0 is the mean annual GST (K), Q_{geo} is the geothermal heat flux (Wm^{-2}), and $k(z)$ is the thermal conductivity ($\text{Wm}^{-1} \text{K}^{-1}$) which may vary with depth. In regions where permafrost exists, latent heat effects due to the freezing and thawing of groundwater play a significant role in the thermal dynamics. Phase change can be accounted for by rewriting the heat equation in terms of enthalpy (Jury & Horton, 2004) as

$$\frac{\partial}{\partial z} \left[k \frac{\partial T}{\partial z} \right] - \frac{\partial h(T)}{\partial t} - S = 0, \quad (2)$$

where $k = k(T)$ is the temperature-dependent bulk thermal conductivity of the material, and $S = S(z, t)$ is a potential external heat source or sink (Wm^{-3}). The volumetric enthalpy (Jm^{-3}) of the soil volume is then defined as

$$h(T) = \overbrace{c(T)(T - T_{\text{ref}})}^{\text{Sensible}} + \overbrace{L\theta_w(T)}^{\text{Latent}}, \quad (3)$$

where $\theta_w(T)$ is the volumetric unfrozen water content ($\text{m}^3 \text{m}^{-3}$), L is the volumetric latent heat of fusion of water (Jm^{-3}), $c(T)$ is the temperature-dependent bulk material heat capacity ($\text{JK}^{-1} \text{m}^{-3}$), and $T_{\text{ref}} = 0^\circ\text{C}$ is the reference temperature set to the freezing point of water at standard conditions. The two additive terms on the right hand side are respectively referred to as sensible and latent energy. We parameterize the bulk thermal properties $k(T)$ and $c(T)$ of the soil volume as simple mixtures of four constituent materials, such that

$$1 = \theta_w + \theta_i + \theta_o + \theta_m, \quad (4)$$

where $\theta_i = \theta_{\text{tot}} - \theta_w$ is volumetric ice content ($\text{m}^3 \text{m}^{-3}$), $\theta_o = (1 - \theta_{\text{tot}})\omega$ is volumetric organic content, and $\theta_m = (1 - \theta_{\text{tot}})(1 - \omega)$ is volumetric mineral content. Here $\theta_{\text{tot}} = \theta_w + \theta_i$ is the total water content, and ω represents the scaled organic fraction of the solid material. Throughout this study, we assume saturated conditions, so θ_{tot} is taken to be equal to the natural porosity of the soil volume. For further details on the parameterizations of the thermal properties, see Groenke et al. (2023); Langer et al. (2024). Note also that Equations 1–3 assume strictly conductive heat transport without any internal heat sources or sinks other than those due to the phase change of water. This model therefore neglects both lateral heat transport as well as advection of heat due to groundwater flow. Boreholes which are known to be significantly affected by such processes are thus not suitable for inversion with this approach.

The constitutive relation $\theta_w(T)$ represents the unfrozen water content as a monotonic function of temperature. For fine-grained soils with high silt or clay content, this function can be highly nonlinear due to the effects of capillary action on the effective freezing point of water in the soil (Koopmans & Miller, 1966). As a result of this nonlinearity, obtaining forward solutions to Equation 2 is generally nontrivial and requires numerical integration with time steps typically ranging from seconds to minutes for high resolution discretizations of the soil volume (≤ 10 cm). To mitigate this, we follow Langer et al. (2024) in using the numerical scheme of Swaminathan and Voller (1992) to efficiently simulate two-phase heat conduction over multiple centuries. We configure the spatial domain of the model to correspond to a 1000 m vertical column extending below the surface of the Earth. The spatial discretization has a resolution of 10 cm in the upper 2.5 m of the ground, where the freeze-thaw dynamics play the largest role, which is then increased non-uniformly to 10 m in the bottom 900 m of the domain. We augment the numerical scheme of Langer et al. (2024) to allow for more realistic forms of $\theta_w(T)$ that can represent the freezing characteristics of common soils when seasonal freezing and thawing is considered. More details on the modified numerical scheme are given in Appendix A.

We represent the GST in our forward model as the sum of three independent components as

$$T(0,t) = T_0 - A \sin\left(\frac{2\pi}{P}(t - t_0)\right) + \sum_{i=1}^N \psi_i(t) \left[\tau_i + \frac{\tau_{i+1} - \tau_i}{t_{i+1} - t_i}(t - t_i) \right], \quad (5)$$

where $T_0 = T(0, t_0)$ is the initial ground surface temperature ($^{\circ}\text{C}$) at the beginning of the simulation period, A is the annual amplitude ($^{\circ}\text{C}$) at the surface, and $P = 1$ yr is the period of the seasonal cycle. In model configurations where the annual cycle is neglected, $A = 0$. Deviations in the GST history from the initial surface temperature T_0 are represented as a continuous piecewise linear function with knots τ_i covering N time segments, where $\psi_i(t)$ correspond to boxcar functions that are zero everywhere outside of the interval $[t_i, t_{i+1})$. We follow Kneier et al. (2018) in setting the endpoints of each segment such that each interval spans a range of $\pm \frac{1}{3}t'$, where t' is the time before the borehole measurement. This loosely reflects the expected loss of temporal resolution that is characteristic of diffusive heat transport (Demezhko & Shchapov, 2001). We set the minimum value of t' to 1 yr since we are only interested in reconstructing GSTs beyond this time horizon.

2.2. Borehole Temperature Data

Temperature profiles $\mathbf{T}(t) = [T(z_1, t), T(z_2, t), \dots, T(z_N, t)]$ consist of a sequence of N temperature measurements along a vertical profile perpendicular to the Earth's surface. Such measurements are typically made by inserting thermistor chains into deep holes drilled into the Earth, often referred to as boreholes. Temperatures can then be measured from boreholes either as point measurements, that is, where the temperature sensors are covered and then left to equilibrate with the subsurface temperature at the time of measurement, or as temporal averages computed from a series of measurements made at regular (sub-daily) intervals over a longer time period, typically at least one annual cycle.

In the latter case, stochastic measurement noise can generally be presumed to be dominated by model error, and seasonal fluctuations in the temperature signal are averaged out over the full profile. In the more common case where \mathbf{T} is a point measurement, temperatures measured at depths above the depth of zero annual amplitude (ZAA) should be discarded for the purposes of GST reconstructions since they are affected by seasonal variations that are typically below the time scale considered in the inversion. Furthermore, measurement error due to the accuracy and resolution limits of the temperature sensor also need to be considered in such cases since fluctuations below these limits should not be allowed to affect the reconstruction. This can be accounted for by setting the error term equal to the sensor resolution (see Section 2.3).

In this work, we consider only the former case of temperature profiles which are computed as temporal averages over at least one full annual cycle. This is the case for both the synthetic experiments, where daily temperature profiles produced by the forward model are averaged over the final simulation year, as well as the experiment using data from an instrumented borehole on Sardakh Island where hourly measurements are available. Note, however, that our method is also readily applicable to point measurements, so long as the aforementioned considerations are taken into account.

2.3. Bayesian Inversion of Ground Temperatures

Bayesian inference provides a natural framework for constraining uncertainty about unknown model parameters using data observed from the system under investigation (Berliner, 2003). For GST reconstruction, we seek to obtain the posterior distribution over the unknown parameters $\phi \in \Phi$ for a particular forward model $\mathcal{M} : \Phi \mapsto T(\mathbf{z}, t_n)$ given some observed temperature profile \mathbf{T} over depths \mathbf{z} at time t_n

$$p(\phi|\mathbf{T}, \mathcal{M}) \propto p(\mathbf{T}|\phi, \mathcal{M})p(\phi|\mathcal{M}) \quad (6)$$

where $p(\phi|\mathcal{M})$ represents the prior distribution over model parameters ϕ for a given forward model \mathcal{M} , and $p(\mathbf{T}|\phi, \mathcal{M}) = \mathcal{N}(\mathcal{M}(\phi), \Sigma_T)$. The model parameters ϕ consist of both the unknowns in Equation 5 (i.e. T_0 , A , and τ) as well as a subset of the unknown parameters required for the heat conduction model such as the soil porosity, solid material thermal conductivity, and the geothermal heat flux at the lower boundary, Q_{geo} . It is important to note that, while we do not generally expect to be able to uniquely determine both the material thermal properties and the GST history simultaneously from a single temperature profile, including them in the posterior distribution still allows us to account for their associated uncertainties in the reconstructed GST histories (Shen et al., 1995; Wang, 1992).

Computing the GST history from Equation 5 over samples from the posterior distribution characterizes the most plausible surface temperature reconstructions after considering the observed temperature profile. One common problem in ground surface temperature reconstruction is enforcing smoothness in the reconstructed temperature history (Hartmann & Rath, 2005). As noted by Hopcroft et al. (2007), the Bayesian approach of computing averages or quantiles over the posterior distribution naturally produces a smoother reconstruction without additional regularization or constraints. However, we observed that neglecting temporal correlation in the prior artificially inflates the spread of the posterior due to the presence of unrealistically large oscillations in independently sampled temperature histories. To mitigate this, we place a multivariate normal prior with Töplitz covariance structure over the temperature offsets. This corresponds to the covariance of a first order autoregressive process where each GST offset is assumed to be correlated with the offset from the previous segment

$$\tau_{i+1} = \rho\tau_i + \epsilon, \quad (7)$$

where $\epsilon \sim \mathcal{N}(0, \sigma^2)$. Since we model the temperature within each segment as a linear ramp between τ_i and τ_{i+1} , it is natural to choose $\rho = \frac{1}{2}$ based on the observation that the average GST within each segment is always $\frac{\tau_{i+1} + \tau_i}{2}$. In all of our experiments, we set $\sigma = 2^\circ\text{C}$ which translates into a prior on temperature deviations with 95% coverage over the interval -4 to 4°C . Note that this does not preclude inference of values outside of this range but naturally requires very strong evidence to override the prior. The initial surface temperature T_0 is assigned a Gaussian prior with mean based on historical air temperatures and variance identical to that of the τ_i parameters.

For the soil parameters (i.e., porosity, mineral thermal conductivity, and organic content in the top layer), we use logit-normal priors centered on the values in the initial stratigraphy with $\sigma = 0.5$; this translates into a prior uncertainty of roughly 5–10% in the constrained parameter space, although the exact deviation depends on the location of the parameter due to the nonlinearity introduced by the logit transform. The log-amplitude, $\log(A)$, is similarly assigned a Gaussian prior with $\sigma = 0.1$ which translates into a variance of roughly $\pm 4^\circ\text{C}$ in the positive constrained space. The mean of the log-amplitude prior can be set for any given site based on the earliest available estimates of air temperature, though it's worth noting that the true GST amplitude will generally be smaller than that of air temperature in cold regions due to the insulating effect of snow cover in the winter (Park et al., 2015). Note that the aforementioned standard deviations are defined in the transformed parameter space and are thus dimensionless.

The posterior distribution in Equation 6 typically has no analytical form for arbitrary priors $p(\phi)$ and nonlinear forward models \mathcal{M} . As a result, numerical sampling methods are required in order to obtain approximate samples from the posterior. Markov Chain Monte Carlo (MCMC) algorithms are generally considered the gold standard of numerical sampling algorithms due to their asymptotic convergence guarantees (Gelman et al., 2013). The method employed by Hopcroft et al. (2007), for example, uses a “reversible jump” variant of MCMC that permits the sampler to vary not only the parameter values but also the number of parameters (i.e., the number of time points in the reconstruction). Such methods are tractable when the forward model has a low computational cost.

Accurately resolving freeze-thaw dynamics in the forward model used in this work, however, makes this impractical at multi-century time scales due to the nonlinearities induced by freezing and thawing.

To circumvent this issue, we use the Ensemble Kalman Sampling (EKS) algorithm of Garbuno-Inigo et al. (2020) as previously outlined by Groenke et al. (2023). EKS is a gradient-free method for approximate Bayesian inference that evolves an initial parameter ensemble as an interactive particle system governed by Langevin dynamics. The algorithm is formulated such that the steady state distribution of the ensemble members corresponds to the posterior distribution in the limit of infinite iterations of the algorithm. Like other ensemble or particle-based sampling algorithms, EKS has the advantage of allowing parallel execution of the model ensemble at each iteration, thus greatly improving efficiency over sequential sampling and optimization methods. To limit the overall computational cost of each experiment, we run EKS for a maximum of 20 iterations with ensembles of size $N_{\text{ens}} = 256$. We specify the residual noise covariance as $\Sigma_T = 4\delta^2 I$ where I is the identity matrix. We found empirically that setting δ to the minimum absolute temperature change in the observed profile generally produced good results and prevented overfitting for both the synthetic and measured temperature profiles.

3. Synthetic Test Cases

3.1. Experiment Setup

We first evaluate our GST inversion method on synthetic test cases where the “true” GST history is known. In order to generate a synthetic temperature profile, we run our forward model over the time period 500–2010 CE forced by air temperatures at the upper boundary taken from the paleoclimate reconstruction of Phipps et al. (2013) for the years 500–1979 and ERA-interim (ERA-I) reanalysis (Dee et al., 2011) for the more recent period of 1979–2010. The paleoclimate reconstruction is based on simulations from the climate system model Mk3Lv1.2. Further details regarding the forcing data are given by Langer et al. (2024). It is important to note that, for the purposes of this experiment, the historical accuracy of the air temperature forcing is not particularly important, as we only aim to produce a semi-realistic temperature profile and GST record that we can use to evaluate the inversion method. We consider a semi-realistic temperature profile for Arctic boreholes to be one that converges to the geothermal gradient with depth (see Equation 1) but is inverted in the upper 30–50 m as a result of rapid surface warming over the last two centuries.

We consider two different synthetic test cases: one based on cold conditions (Section 3.2) and one based on warm conditions (Section 3.3). This is motivated by recent findings that the thermal response of cold versus warm permafrost to climate change often differ substantially (Groenke et al., 2023; Nicolsky & Romanovsky, 2018) as well as by the hypothesis that latent heat effects will likely be more dominant in regions where permafrost has temperatures closer to 0°C. We select the Lena River Delta in northeastern Siberia as the prototype for cold conditions since it lies well within the region characterized by our working definition of cold permafrost (Figure 1a). For the warm prototype, we select a region east of the James Bay in western Quebec where previous studies indicate that significant permafrost thaw has likely occurred (Figure 1b). By this definition, roughly two-thirds of permafrost in the northern hemisphere can be considered “warm” which underscores the importance of correctly representing such regions in geothermal climate reconstructions.

For each synthetic test case, we apply constant freezing and thawing degree-day factors (Groenke et al., 2023; Lunardini, 1978) to the air temperatures in order to roughly approximate the thermal offset between near-surface air temperature and GST due to snow, vegetation, and other factors. We initialize the forward model with a steady state temperature profile corresponding to a fixed initial surface temperature T_0 and geothermal heat flux $Q_{\text{geo}} = 53 \text{ mW m}^{-2}$. We select 1700–2010 CE as the inversion period with the first 1200 year period (500–1700 CE) of the forward run discarded as spin-up. The “observed” temperature profile data sets are then produced by taking the MAGT profile over 10 depths ranging from 1 to 100 m over the final simulation year.

We use a simple, three-layer soil stratigraphy (Table 1) in the forward model which consists of a 1 m thick organic rich layer (A Horizon) followed by a 19 m thick medium porosity subsoil layer (B Horizon) and low-porosity layer representing a combined substratum and bedrock layer (C + R Horizon) thereafter (Jahn et al., 2006). In order to investigate the impact of freeze-thaw dynamics on the reconstruction, we use a freezing characteristic curve where approximately 8% of the pore water remains unfrozen at -10°C . This is a typical freezing characteristic for soils with high silt or clay content (Carsel & Parrish, 1988; D. W. Riseborough, 2002; Ren & Vanapalli, 2019). While such soils are not necessarily representative of all the soil types actually found in the

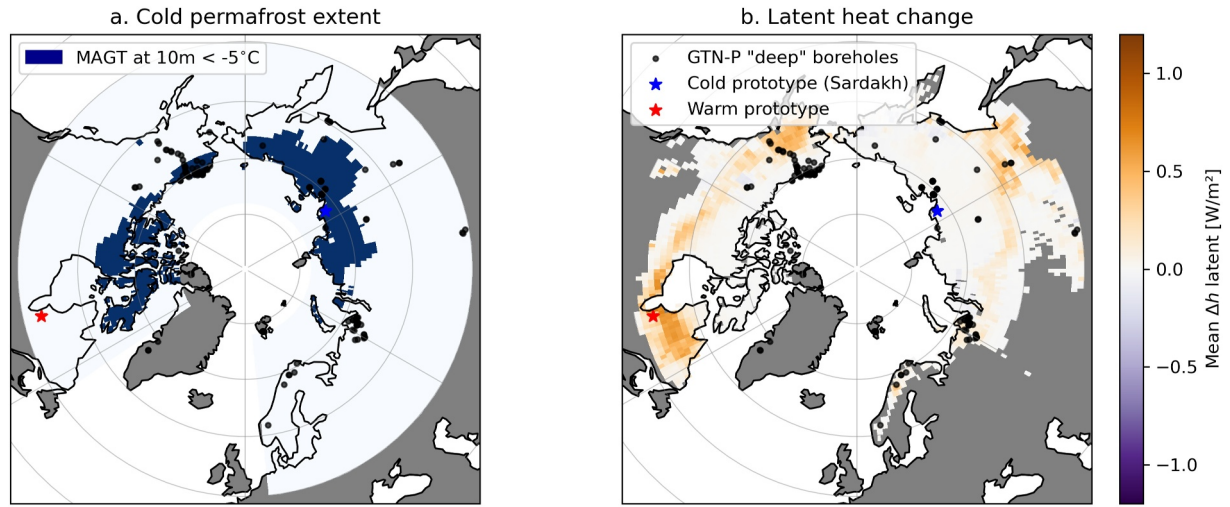


Figure 1. Maps showing the prototype warm and cold locations used by the synthetic experiments in this study, as well as GTN-P boreholes deeper than 50 m, overlain on a map of “cold” permafrost extent (a), here defined as areas where simulated mean annual ground temperatures are below -5°C at 10 m depth. We calculate the spatial extent of cold permafrost, by this definition, to be approximately 34.1% of the total area considered here. The second panel (b) shows total latent heat change as estimated by Nitzbon et al. (2023) for the time period 1980–2018. Higher latent heat change generally indicates more thaw.

study regions considered here, they represent an end-member case in which we would expect freeze-thaw dynamics to be most likely to affect the observed temperature profiles even at temperatures well below the nominal freezing point of water.

For each data set, we compare four different parameterizations of the forward model used in the inversion:

1. *Homogeneous soil without seasonal thaw* (FW1L). The soil stratigraphy is misspecified as a homogeneous medium with all material and thermal properties invariant with depth. No seasonal cycle is applied to the upper boundary (i.e. $A = 0$) thereby excluding the active layer. The idealized “free water” freezing characteristic (see Appendix A) is used in place of a soil freezing characteristic. As a result, freezing and thawing at the surface will not occur unless the average GST over the reconstruction period exceeds the melting point $T_m = 0^{\circ}\text{C}$.
2. *Three-layer soil without seasonal thaw* (FW3L). This configuration is the same as the FW1L but using the “true” three-layer soil stratigraphy given in Table 1.
3. *Three-layer sandy soil with seasonal thaw* (SS3L). Three-layer soil stratigraphy with seasonal temperature variation applied to the GST. The van Genuchten parameters (van Genuchten, 1980) governing the shape of the soil freezing characteristic curve are intentionally misspecified using typical values for a sandy soil. In sandy soils, freezing occurs much earlier when temperatures fall below 0°C .
4. *Three-layer clay soil with seasonal thaw* (CS3L). This configuration corresponds to the ground truth forward model with a simplified upper boundary following Equation 5. Note, however, that the soil parameters in each layer are still varied, so each sampled model realization is generally not identical to the ground truth forward model.

Table 1
Three-Layer Soil Stratigraphy Used for the Synthetic Forward Runs

Layer	Depth	$\theta_{\text{tot}} \times 100$	$\omega \times 100$	k_m
1	0.0	50 ± 10	30 ± 10	2.8 ± 5
2	1.0	35 ± 10	1	3.1 ± 5
3	20.0	5 ± 5	0	3.5 ± 5

Note. Soil properties are treated as homogeneous within each layer. Here θ_{tot} refers to the total water/ice content, presumed equal to porosity (m^3m^{-3}), ω to the organic solid fraction (m^3m^{-3}), and k_m to the thermal conductivity ($\text{Wm}^{-1}\text{K}^{-1}$) of the mineral constituent. Uncertainties refer to the (approximate) standard deviations of the prior.

Comparing configurations 1 (FW1L) and 2 (FW3L) allows us to quantify the impact of neglecting spatial heterogeneity in the soil properties while comparing configurations 3 (SS3L) and 4 (CS3L) allows us to assess the impact of misspecifying the soil freezing characteristic. We can additionally compare configurations 2 (FW3L) and 3 (SS3L) in order to quantify the impact of excluding seasonal freeze-thaw effects.

In each experiment, the set of model parameters considered in the inversion includes the initial GST T_0 , the geothermal heat flux Q_{geo} , and the 10 GST offsets at geometrically spaced intervals between 1500 and 2010 (see Section 2.1). For the cases where seasonal thaw is considered, the annual amplitude is also included as a parameter. In the homogeneous soil configuration, the porosity and mineral thermal conductivity are varied as

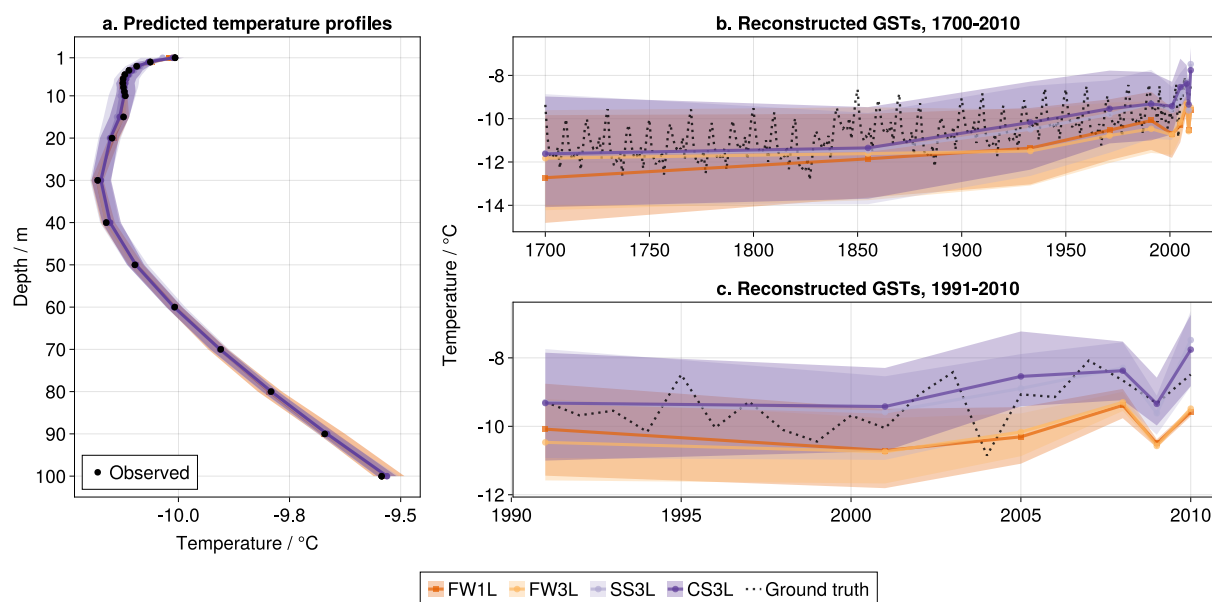


Figure 2. Reconstructed ground surface temperatures for synthetic borehole data in cold conditions (a) along with the corresponding predicted temperature profiles (b). The dotted black line shows the “true” mean annual ground surface temperature history produced by running the forward model with air temperature forcing from northeastern Siberia (E 127° N 72°). The solid colored lines correspond to the median and the shaded regions to the 90% highest density interval over the posterior ensemble.

parameters, and in the three-layer soil stratigraphy, these parameters are varied independently within each of the layers for a total of six additional parameters. Since the primary goal of these experiments is to evaluate differences in the reconstructed GST histories rather than recover the soil parameters, we center the parameter priors for the three-layer model configurations on the true values used in the forward model (Table 1) to avoid introducing a priori biases into the inversion.

3.2. Cold Conditions

For the first experiment, we use a data set generated by the forward model forced by air temperatures from a region in northeastern Siberia (E 127° N 72°) at the edge of the Laptev Sea. We use freezing and thawing degree day factors of 0.7 (fairly cold, low to moderate snow cover) and 0.9 (minimal insulation from vegetation) respectively. The region lies within the continuous permafrost zone and is characterized by historically low mean annual air temperatures (−16°C for the pre-industrial period 1500–1850 CE). As a result, MAGT can reach −10°C or lower even at depths well below the active layer (Romanovsky et al., 2007). The average GST in the ground truth simulation increased by 2.4°C over the study period (1700–2010 CE) with active layer thickness (ALT) increasing from roughly 40–60 cm over the same time frame.

All four model configurations are able to produce temperature profiles which fit well to the synthetic temperature profile (Figure 2a) with the mean absolute error and full 90% highest density interval <0.05°C in all cases (Table 2). We note that the posterior predicted ground temperatures from all three of the model configurations which use the “true” three-layer soil stratigraphy are nearly identical, whereas the homogeneous soil variant has larger uncertainty below 30 m depth. This can be attributed to the model’s inability to account for heterogeneity in the soil thermal properties, thereby producing biases in the predicted temperature profiles. The median predicted temperature profile nevertheless shows good agreement. This seems to indicate that the temporal variations in the inverted GSTs can compensate for such biases arising from misspecification of the soil thermal properties. This is consistent with the findings of Shen et al. (1995) who assessed the impact of heterogeneous thermal properties on the reconstructions.

The reconstructed GST histories for each model configuration (Figure 2b) are largely consistent in terms of the relative warming over each reconstruction period. There are, however, two noteworthy discrepancies between the model variants with and without seasonal thaw. The first and most obvious difference is the constant shift of approximately 1°C which arises due to the thermal offset from freezing and thawing of the active layer. The

Table 2

Summary Statistics for Evaluating the Inversion Produced by Each Model Configuration Under Cold Versus Warm Conditions: Ground Surface Temperatures, Ground Surface Temperature (GST) Reconstruction Bias, Mean Absolute Error in the Predicted Temperature Profiles, and Pearson Correlation With the True GST History Averaged Over the Reconstruction Intervals

Model	Cold			Warm		
	Rec. bias (°C)	Pred. MAE (°C)	Corr.	Rec. bias (°C)	Pred. MAE (°C)	Corr.
FW1L	-0.95 ± 0.16	0.01 ± 0.0	0.82 ± 0.13	-2.59 ± 0.26	0.04 ± 0.01	0.71 ± 0.15
FW3L	-0.91 ± 0.14	0.0 ± 0.0	0.80 ± 0.17	-2.27 ± 0.23	0.06 ± 0.01	0.67 ± 0.14
SS3L	0.0 ± 0.29	0.02 ± 0.03	0.86 ± 0.10	-0.99 ± 0.52	0.04 ± 0.02	0.83 ± 0.10
CS3L	0.14 ± 0.34	0.01 ± 0.02	0.87 ± 0.09	-0.70 ± 0.52	0.04 ± 0.02	0.87 ± 0.09

Note. Uncertainties correspond to the standard deviation over the posterior ensemble ($N = 256$).

second difference is in the inferred ground surface temperature for the last reconstruction period of 2009–2010; both of the model variants with seasonal thaw (SS3L and CS3L) overestimate the warming in the final year by 0.8°C and 1.3°C respectively (Figure 1c). This is likely due to the GST parameterization assuming that the seasonal amplitude remains stationary over time. Closer inspection of the ground truth air temperature forcing data shows an asymmetric increase in the decadal average of minimum annual air temperature of 4.1°C since 1950 versus an increase of 3.8°C in maximum annual air temperature. Since this winter warming effect cannot be captured by a GST parameterization with static annual amplitude, the result is a positive bias in the estimated increase in the mean.

Both of the models which exclude seasonal thaw, thereby neglecting latent heat effects, produce GSTs with cold biases of $-0.95 \pm 0.02^\circ\text{C}$ (FW1L) and $-0.91 \pm 0.01^\circ\text{C}$ (FW3L) compared to much smaller biases of $0.0 \pm 0.3^\circ\text{C}$ and $0.1 \pm 0.3^\circ\text{C}$ in the sand and clay models, respectively (Table 2). While it may initially appear somewhat surprising that the inversion using the ground truth model configuration (CS3L) has a larger bias than the SS3L variant, it is important to note that the difference of approximately 0.1°C is well within the uncertainty bounds for both inversions. The cold bias in the FW1L and FW3L model variants can be at least partially explained by the thermal offset in MAGT typically observed in the active layer. We note again that, when the active layer is neglected in the model, its thermal offset is not present, and the reconstructed GSTs effectively represent the TTOP (Lachenbruch & Marshall, 1986).

3.3. Warm Conditions

For this experiment, we use air temperatures from western Quebec, east of the James Bay (W 77° N 53°) to force the forward model. The region lies outside of the continuous permafrost zone and is characterized by historical mean annual air temperatures of -6°C for the pre-industrial time period of 1500–1850. The average GST in the ground truth simulation increased by 4.9°C over the study period (1700–2010 CE) with ALT increasing substantially from 80 to 350 cm over the same time frame.

We find that the inversion method is again able to produce temperature profiles that are in good agreement with the simulated observations (Figure 3a) with the mean absolute prediction error $<0.1^\circ\text{C}$ for all four model configurations (Table 2). We note, however, that unlike in the cold experiment, the two soil models which incorporate seasonal freeze-thaw have a larger spread in the predicted temperature profiles. This is likely due to the sensitivity of two-phase heat transport to uncertainty in soil parameters such as porosity, which directly determines the amount of water/ice which undergoes freezing and thawing. This is the case for all subzero temperatures, but the effects are stronger at temperatures closer to the freezing point of water, where the constitutive relation between temperature and unfrozen water content becomes increasingly nonlinear.

Like in the cold experiment, the reconstructed GSTs for both model configurations which neglect phase change (FW1L and FW3L) have significant cold biases ($-2.6 \pm 0.3^\circ\text{C}$ and $-2.3 \pm 0.2^\circ\text{C}$ respectively) when averaged over the study period (Figures 3b and 3c and Table 2). Since we use the same ground truth stratigraphy setup in both experiments, we can infer that the larger magnitude of the bias in this case can only be explained by the deeper active layer, which naturally results in a larger offset between the ground surface and the top of the permafrost. As permafrost thaws and the active layer deepens, this offset becomes larger, which may explain the

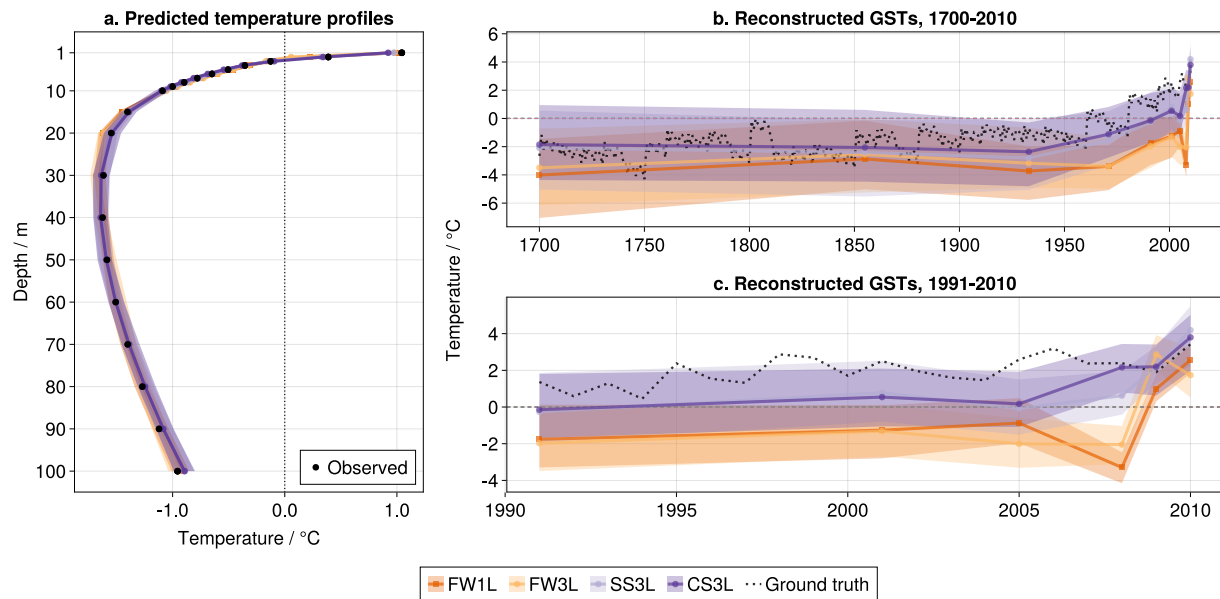


Figure 3. Reconstructed ground surface temperatures for synthetic borehole data in warm conditions (a) along with the corresponding predicted temperature profiles (b). The dotted black line shows the “true” mean annual ground surface temperature history produced by running the forward model with air temperature forcing from western Quebec, east of the James Bay (W 77° N 53°). The solid colored lines correspond to the median and the shaded regions to the 90% highest density interval over the posterior ensemble.

minimal change in the early 20th century GSTs from both of these model configurations (Figure 3b). In contrast, the inversion for the clay soil model (CS3L) accurately recovers the warming trend over both the 19th and 20th centuries, though there is still a significant cold bias of $-0.7 \pm 0.5^\circ\text{C}$. This could be explained by two factors: (a) biases in the thermal offset of the active layer due to the changes in the phase and/or amplitude of the seasonal cycle and (b) short-term warming events in the forcing data that are below the time scale resolvable by the GST parameterization.

All four models consistently reproduce the warming trend of the late 20th century, though the models excluding seasonal thaw (FW1L and FW3L) tend to slightly overestimate the rate of warming. Both of these models also infer a spurious cooling pattern and subsequent large jump in the GST ($>3^\circ\text{C}$) for the last two reconstruction periods (2007–2009 and 2009–2010) in order to fit the uppermost depths in the temperature profile at 1 and 2 m (Figure 3c). This is because the MAGT at these depths are significantly higher due to being in the active layer at the end of the study period. Since both of these model configurations do not include seasonal thaw, they are not able to represent the active layer, and thus the only way to fit these points is by dramatically increasing the GST in the most recent years. This effect could be mitigated to some extent by simply removing these points from the inversion and setting the upper boundary of the soil domain to a depth that is assumed to be well below the active layer throughout the study period. However, this requires ALT for the site or region to be known a priori and precludes direct comparison with other GST records from observations or land surface models that are able to represent freezing and thawing of the active layer.

4. Inversion of Borehole Data From Sardakh Island

We additionally evaluate our method on real-world borehole data from a 100 m borehole on Sardakh Island which was drilled in 2009 (Kneier et al., 2018). Sardakh Island lies in the southern part of the Lena River Delta in northeastern Siberia and is characterized by very long and cold winters with temperatures reaching -45°C and below. The site lies within the region covered by the forcing data described in Section 3.2 and thus can be assumed to have likely experienced similar pre-industrial mean annual air temperatures of roughly -16°C . Recent analyses of air temperatures at the nearby Samoylov Island station (Boike et al., 2019), which lies roughly 50 km southwest of Sardakh, show significant warming of at least $0.1^\circ\text{C yr}^{-1}$ over the last two decades with recent mean annual air temperatures ranging from -12 to -8°C (Groenke et al., 2023).

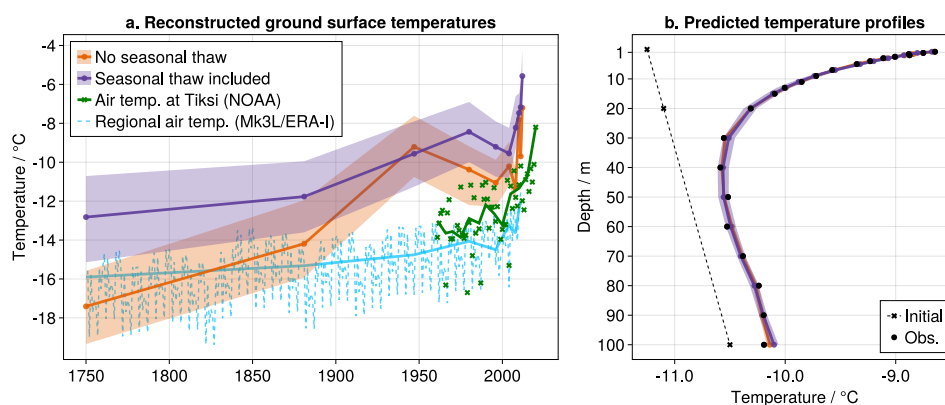


Figure 4. Reconstructed ground surface temperatures from the 100 m borehole on Sardakh Island (a) along with the corresponding predicted temperature profiles (b) both including and excluding seasonal temperature variations at the surface. The dashed blue line in panel (a) represents the air temperature forcing of Langer et al. (2024) for the region (see Section 3.2) over the full study period; the corresponding solid blue line shows the same data averaged over the reconstruction intervals. The green crosses show annual average air temperatures measured from the nearby NOAA meteorological station at Tiksi with the solid line showing half-decadal averages. The black dots in panel (b) are mean annual ground temperatures at each depth for the period 2011–10–1 to 2012–10–1. The dashed line shows the upper part of the temperature profile used to initialize the forward model in the year 1600 CE.

We use the same underlying data set and stratigraphy information for the site as published previously by Kneier et al. (2018). We select, however, the slightly more recent time frame of 2011–2012 instead of 2010–2011 due to the data record having fewer gaps after cleaning and quality control. We discard temperature measurements above 1 m depth since these are likely to be affected by land surface processes that our model cannot resolve. We also use a condensed, eight-layer version of the soil stratigraphy (Table B1) that includes a half meter thick organic layer at the top of the soil profile. Like in the synthetic experiments, we allow the porosity and mineral thermal conductivity to vary as parameters in each of these layers.

The reconstructed GST histories and predicted temperature profiles, both including (purple) and excluding (orange) seasonal freezing and thawing, are shown in Figure 4. The inversions from both model configurations indicate substantial warming of 5–9°C over the last two centuries. Furthermore, consistent with the results shown in Sections 3.2 and 3.3, the model variant excluding freezing and thawing at the upper boundary generally underestimates GSTs due to the thermal offset of the active layer. In this case, this offset does not appear to be entirely constant over the 160 yr time period. This may be in part due, however, to the deepest temperature measurement at 100 m depth which appears unusually cold in comparison to the geothermal gradient. This is discussed further in Appendix B.

Both variants also indicate a cooling period during the latter half of the 20th century though they disagree about the timing and magnitude of this cooling. The first reconstruction excluding seasonal thaw (Figure 4a) suggests that GSTs initially peaked around 1950 before cooling by roughly 1.5°C by the end of century. The second reconstruction that includes seasonal thaw indicates the onset of cooling to have started in the mid-1970s. Observed air temperatures from the nearby NOAA station at Tiksi appear to suggest that this cooling may have started even later (early to mid 1980s), though there are two unusually cold years (below –16°C) in the two decades prior (1966 and 1979). This discrepancy could be due to the fact that the reconstructions are limited in their capacity to resolve the timing of past changes by the fixed time intervals. The half-decadal averaged air temperatures at Tiksi show a decrease of roughly 1°C from 1986 to 1995 which is consistent with the reconstruction that includes seasonal thaw. This timing is also roughly consistent with previous reconstructions from the same borehole (Kneier et al., 2018). Ice core reconstructions from the Russian high Arctic have also indicated similar 20th century cooling, though the timing varies across samples (Fritzsche et al., 2005; Opel et al., 2013).

The reanalysis air temperature record for the region shown by the blue line in Figure 4a (Langer et al., 2024) also largely agrees with the timing of the cooling indicated in the second reconstruction, although the long-term average (solid line) suggests a smaller magnitude of roughly 0.2°C. The model variant excluding seasonal thaw is able to resolve the short-term temperature fluctuation during the mid 2000s seen in the reanalysis air

temperature record, while the model variant including seasonal thaw does not. This may be due to the freezing and thawing of the active layer effectively damping out this fluctuation in the forward model, reducing the apparent effect size of these GSTs in the inversion. This hypothesis is further supported by the observation that the first model variant without seasonal thaw accurately predicts the ground temperature at 30 m depth while the second model variant with seasonal thaw has a warm bias of roughly 0.05°C which may be due to this cooling event not being resolved.

5. Discussion

Both our synthetic and real-world test cases demonstrate that latent heat effects have a significant impact on the inverted GSTs due to the impacts of freezing and thawing on the thermal dynamics of the soil. This is especially the case in warmer regions where permafrost temperatures are higher than -5°C and ALT varies significantly over time. However, our results also indicate that, under cold conditions where ALT remains relatively stable, the impact of seasonal freeze-thaw on GST reconstructions is limited primarily to a quasi-constant shift due to the thermal offset of the active layer. Long-term warming at the surface may also be underestimated when neglecting the active layer since energy being consumed as latent heat is not accounted for. Under such conditions, classical inversion methods that neglect latent heat effects could still be used so long as the inverted upper boundary temperatures are carefully interpreted as TTOP and are not directly compared to measured or simulated ground temperatures within or above the active layer. Latent heat effects can also generally be ignored in boreholes where the porosity of the solid material is lower than 5% (Mottaghy & Rath, 2006). However, in the more common high porosity permafrost soils where the active layer is likely to play a significant role, existing methods that ignore seasonal thawing of the active layer should not be used, as they will produce physically incoherent inversions due to the non-stationary position of the upper boundary (i.e., the permafrost table). Our method provides a viable solution to this problem by directly accounting for the seasonal freezing and thawing of the active layer in the forward model and representation of the GST, thus making it more suitable for boreholes in frozen soils. We note also that our approach has the advantage of being broadly applicable to arbitrarily complex forward models of heat (and potentially water) flow, so long as the numerical scheme allows for large enough time steps to make simulations on time scales of centuries to millennia feasible within a given computational budget.

Despite the advantages of our proposed method, there are some important caveats to consider. First, the EKS algorithm that we use for inference is still relatively costly, requiring a total of 5,120 forward model evaluations over the full inversion period (310 years for the synthetic experiment); that is, 20 iterations of an ensemble of size $N_{\text{ens}} = 256$. Even with the (relatively) efficient forward model which required 5–10 min of wall clock execution time per forward model evaluation, this translated into each iteration taking roughly 20–30 min on a compute cluster with a 64-core AMD EPYC 7742 processor (256 vCPUs) and 1 TB of memory. Thus, reconstructions spanning multiple millennia may be prohibitively expensive depending on available compute resources. Future work might therefore consider alternative inference algorithms that employ emulators or reduced-order models to reduce this cost, for example, the “calibrate, emulate, sample” method of Cleary et al. (2021).

Second, our formulation of the GST currently assumes the annual amplitude to remain fixed over the full inversion period. This is a significant source of potential uncertainty since there is ample reason to believe that winter warming has been stronger than summer warming in many Arctic regions (Meyer et al., 2015; Rantanen et al., 2022). While it is theoretically possible within our framework to parameterize the GST amplitude as a time-varying function in addition to the long-term mean, this would greatly increase both the size and the complexity of the resulting inverse problem. As such, we consider the constant amplitude assumption to be a reasonable first order approximation.

Third, our approach uses a fixed length parameterization of the GST function; that is, we do not consider the impacts of varying the size and number of time segments in the reconstruction. This constitutes a significant source of unquantified uncertainty since the timing of each change point has a substantial impact on the observed temperature profile. One possible improvement could be to combine our forward thermal model of permafrost with the reversible-jump Markov Chain Monte Carlo approach of Hopcroft et al. (2007). There are significant computational challenges in doing so, however, since such algorithms tend to require tens of thousands of (sequential) iterations to converge, which is prohibitively difficult given the much higher resolution of our forward model.

Another natural continuation of this work would be to apply our method to a circumpolar or global data set such as the GTN-P (Biskaborn et al., 2015) or the Xibalbá database (Cuesta-Valero et al., 2022). This would enable larger scale GST reconstructions across the cryosphere. However, deep boreholes, here defined as those that extend to depths of at least 50 m below the surface, are relatively rare in Arctic and subarctic regions. This is especially the case in many of the warmer areas where permafrost is likely to be rapidly thawing (see Figure 1b). Boreholes with accessible temperature records spanning both the active and deeper permafrost layers, as well as metadata describing the soil properties, are unfortunately even rarer. Furthermore, despite the development of borehole metadata networks such as GTN-P, ground temperature data from existing boreholes are generally not readily accessible at a global scale.

There is, therefore, an urgent need for a global campaign to install additional deep boreholes in regions where limited historical climate data are available as well as for an improved global database of temperature profiles from permafrost boreholes. Novel reconstruction methods such as ours significantly increase the value of such efforts since, in addition to providing information about the present and future thermal state of permafrost, these data can also provide valuable information about historical climate change predating available observational records. For the time being, however, significant challenges remain in conducting a robust, global scale reconstruction of historical GSTs in permafrost regions from borehole temperature measurements.

6. Conclusions

In this work, we presented a novel method for reconstructing historical ground surface temperatures (GST) from permafrost boreholes using Bayesian inversion of an efficient numerical model of two-phase heat transport in permafrost soils. There are two key innovations in our work: (a) this is the first study to systematically analyze the impact of seasonal freezing and thawing on GST reconstructions in both cold and warm permafrost environments, and (b) our proposed method is, to the best of our knowledge, the first method for geothermal climate reconstruction that is widely applicable to boreholes in regions underlain by permafrost. We demonstrated through experiments with both synthetic and real-world data that latent heat effects due to seasonal thawing and refreezing of the active layer can have a substantial impact on the reconstructed GST histories, especially in warmer regions where permafrost is most likely to be thawing. This implies that such effects should not be ignored in studies which aim to reconstruct surface temperatures from boreholes in regions where permafrost currently is or previously was present. Our work highlights the need for further collection and aggregation of borehole data in cold regions in order to facilitate such reconstructions and improve our understanding of the past, present, and future evolution of permafrost.

Appendix A: Numerical Details of the Forward Model

The permafrost thermal modeling approach of Langer et al. (2024) is based on the numerical scheme of Swaminathan and Voller (1992). This approach solves the discretized partial differential equation using a first-order, backwards Euler time stepping scheme where the energy state at each time step is solved iteratively:

$$h_i^{j+1} = h_i^j + \frac{\partial h}{\partial T_i^j} \left[T_i^{j+1} - h^{-1}(h_i^j) \right] \quad (\text{A1})$$

where j and i refer to the iteration and discretized grid cell indices respectively. The initial iteration h_i^0 is set to the energy state from the previous time step. The temperature field at each iteration is solved by linearizing the diffusion Equation 2 at the next time point t and solving the linear system for \mathbf{T}^{j+1} :

$$A\mathbf{T}^{j+1} - \frac{\partial h}{\partial \mathbf{T}^j} \frac{\mathbf{T}^{j+1} - \mathbf{T}^j}{\Delta t} - \frac{h(\mathbf{T}^j) - \mathbf{h}^0}{\Delta t} - \mathbf{b} = 0 \quad (\text{A2})$$

where \mathbf{T}^j is the discretized temperature state vector at iteration j , A is the tridiagonal diffusion matrix, \mathbf{h}^0 is the previous energy state, $\Delta t = 24$ hr is the time step size, and \mathbf{b} is a forcing term appropriately augmented with the corresponding Dirichlet or Neumann boundary conditions at the current time step.

Key to this approach is the invertible enthalpy-temperature relation, $h(T_i)$, which corresponds to the general enthalpy function given by Equation 3. For simplicity, Langer et al. (2024) use the so-called “free water” freezing characteristic which defines the unfrozen water content θ_w in terms of enthalpy:

$$\theta_w(h_i) = \begin{cases} \theta_i^{\text{tot}} & h_i > L\theta_i^{\text{tot}} \\ \frac{h_i}{L} & 0 \leq h_i \leq L\theta_i^{\text{tot}} \\ 0 & h_i < 0 \end{cases} \quad (\text{A3})$$

where θ_i^{tot} is the total volumetric water and ice content of the i 'th soil volume, typically equal to the porosity under saturated conditions. Temperature is then correspondingly determined according to the inverse enthalpy relation:

$$h^{-1}(h_i) = \begin{cases} \frac{(h_i - L\theta_i^{\text{tot}})}{C_i} & h_i > L\theta_i^{\text{tot}} \\ 0 & 0 \leq h_i \leq L\theta_i^{\text{tot}} \\ \frac{h_i}{C_i} & h_i < 0 \end{cases} \quad (\text{A4})$$

where $C_i = C(\theta_i)$ is the volumetric heat capacity at grid cell i , and here $\theta_i = \theta_w(h_i)$ as defined above. The free water freezing characteristic corresponds to the idealized case of phase change in pure water. We also use this formulation in the model variants which exclude seasonal thaw.

As discussed in Section 2.1, realistic representations of the freezing and thawing of water in porous media such as soils are complicated by the presence of capillary action which effectively lowers the freezing point of water in the soil pores. In order to account for these effects in the implicit integration scheme described above, it is necessary to define an inverse function for Equation 3. While no analytical inverse function is generally available, temperature can be recovered by solving a nonlinear system for T_i in the i 'th grid cell:

$$\frac{h_i - L\theta_w(T_i)}{C_i} - T_i = 0 \quad (\text{A5})$$

where $C_i = C(T_i)$ is the temperature dependent volumetric heat capacity. For computational efficiency, we precalculate this inverse function over a large temperature range (-50 to 50°C) within each stratigraphy layer using an adaptive linear interpolation scheme with an error tolerance of 10^{-4} or 0.01%. In order to ensure good convergence of the iterative scheme (A1), we found it necessary to reduce the integration time step Δt to 12 hr.

Our scheme is generally agnostic to the choice of freezing characteristic, $\theta_w(T)$, so long as the resulting enthalpy-temperature relation is monotonic and has a unique solution for any given energy state. For the synthetic experiments, we use the freezing characteristic described by Painter and Karra (2014) with van Genuchten (1980) parameters $\alpha = 0.145 \text{ cm}^{-1}$ and $n = 2.68$ for the prototypical sandy soil case and $\alpha = 0.02 \text{ cm}^{-1}$ and $n = 1.31$ for the clay soil case (Carsel & Parrish, 1988). For the Sardakh Island borehole, in order to be consistent with the previous analysis of Kneier et al. (2018), we use instead the empirical function derived by Langer et al. (2011) for a nearby site on Samoylov Island.

Appendix B: Additional Details for Sardakh Island Inversion

The soil stratigraphy used for the Sardakh Island borehole inversion is given in Table B1. We derived this stratigraphy manually based on the details provided in the supplement of Kneier et al. (2018) regarding the Sardakh Island borehole. The eight layers correspond roughly to the lithology of the region, and the specific values for the soil parameters in each layer are taken from the inversion results published in the same work.

The posterior densities of the porosity and thermal conductivity parameters in each layer are shown in Figure B1. There is relatively minimal deviation from the priors except in the porosity of the top organic layer which is poorly

Table B1
Soil Stratigraphy Used for the Sardakh Island Borehole Inversion

Layer	Depth [m]	$\theta_{\text{tot}} \times 100$	$\omega \times 100$	k_m
1	0.0	80 ± 10	25 ± 10	2.5 ± 0.5
2	0.5	50 ± 10	1	2.5 ± 0.5
3	9.0	20 ± 10	0	2.5 ± 0.5
4	13.0	10 ± 5	0	3.0 ± 0.5
5	18.0	20 ± 10	0	2.5 ± 0.5
6	30.0	5 ± 5	0	2.5 ± 0.5
7	50.0	5 ± 5	0	1.0 ± 0.5
8	80.0	10 ± 5	0	2.5 ± 0.5

Note. Soil Parameters are Assumed to Be Homogeneous Within Each Layer. Here θ_{tot} Refers to the Total Water/Ice Content, Presumed Equal to Porosity ($\text{m}^3 \text{m}^{-3}$), ω to the Organic Solid Fraction, and k_m to the Thermal Conductivity ($\text{W m}^{-1} \text{K}^{-1}$) of the Mineral Constituent. Uncertainties Refer to the (Approximate) Standard Deviations of the Prior.

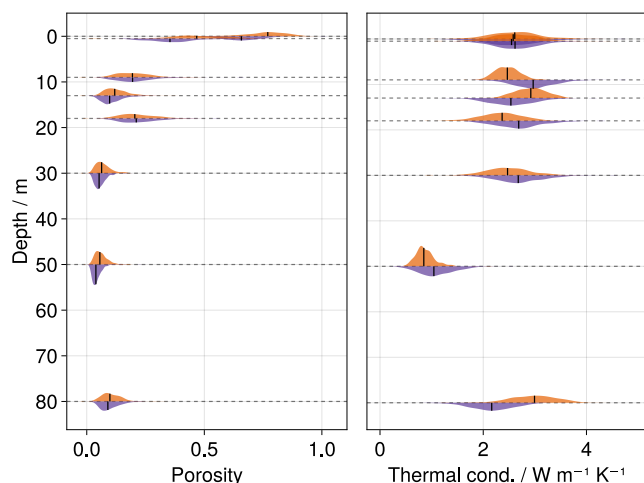


Figure B1. Posterior densities for the porosity and thermal conductivity parameters in each stratigraphy layer. The top (orange) density in each layer corresponds to the model without seasonal thaw, while the bottom (purple) density corresponds to the model with seasonal thaw included.

constrained given that we do not include temperature measurements above 1 m. There are some slight deviations between the two model variants, for example, in the thermal conductivities of layers 3–5. The posterior densities for the variant with seasonal thaw appear to have shifted (increasing in layer 3 and decreasing in layer 4) which is likely to compensate for the impacts of freezing and thawing on the thermal properties of the upper layers. In the bottom-most layer, the posterior density for the first model variant (excluding seasonal thaw) indicates a higher thermal conductivity which would result in a smaller geothermal gradient. This is consistent with the smaller bias in the predicted temperature profiles shown in Figure 4b. The reason for the decrease in the posterior estimate of this conductivity for the model variant with seasonal thaw is, however, less clear. It could be that this is a compensating effect for the model having a slight cold bias at the 80 m sensor, or it may simply be an artifact of the sampling method failing to adequately adjust these parameters. The inclusion of the annual signal increases the difficulty of the optimization problem since it adds an additional parameter (i.e., the seasonal amplitude) and makes the response of the near-surface ground temperatures to the GST signal more nonlinear.

Data Availability Statement

The data and code repository used to generate the results in this work is available on Zenodo (Groenke, Langer, & Miesner, 2024). The code for the forward model, CryoGrid.jl, is available as open source software on both GitHub

and Zenodo (Groenke, Nitzbon, & Langer, 2024). The historical air temperature forcing data used in the synthetic experiments can be downloaded from Zenodo (Langer et al., 2022a). The model outputs from Nitzbon et al. (2023) and Langer et al. (2024) used in Figure 1 are also available on Zenodo (Langer et al., 2022b). Air temperature data from Tiksi can be obtained directly from the NOAA Climate Data Center (NOAA National Centers of Environmental Information, 1999).

Acknowledgments

Brian Groenke (BG) acknowledges the funding and support of the Helmholtz Einstein International Berlin Research School in Data Science (HEIBRiDS) as well as the German Academic Exchange Service (DAAD). BG additionally acknowledges the support of the Environmental Research Centre Leipzig in cooperation with the Center for Scalable Data Analytics and Artificial Intelligence (ScaDS.AI). Open Access funding enabled and organized by Projekt DEAL.

References

- Alifanov, O. M. (2012). *Inverse heat transfer problems* (1st ed., pp. 0741–5877). Springer Science and Business Media. <https://doi.org/10.1007/978-3-642-76436-3>
- Beck, A. E., & Judge, A. S. (1969). Analysis of heat flow data—I detailed observations in a single borehole. *Geophysical Journal International*, 18(2), 145–158. <https://doi.org/10.1111/j.1365-246X.1969.tb03558.x>
- Beltrami, H. (1996). Active layer distortion of annual air/soil thermal orbits. *Permafrost and Periglacial Processes*, 7(2), 101–110. [https://doi.org/10.1002/\(SICI\)1099-1530\(199604\)7:2<101::AID-PPP217>3.0.CO;2-C](https://doi.org/10.1002/(SICI)1099-1530(199604)7:2<101::AID-PPP217>3.0.CO;2-C)
- Benestad, R. E., Erlandsen, H., Mezghani, A., & Parding, K. M. (2019). Geographical distribution of thermometers gives the appearance of lower historical global warming. *Geophysical Research Letters*, 46(13), 7654–7662. <https://doi.org/10.1029/2019GL083474>
- Berliner, L. M. (2003). Physical-statistical modeling in geophysics. *Journal of Geophysical Research*, 108(D24). <https://doi.org/10.1029/2002JD002865>
- Biskaborn, B. K., Lanckman, J.-P., Lantuit, H., Elger, K., Streletskiy, D. A., Cable, W. L., & Romanovsky, V. E. (2015). The new database of the global terrestrial network for permafrost (GTN-P). *Earth System Science Data*, 7(2), 245–259. <https://doi.org/10.5194/essd-7-245-2015>
- Biskaborn, B. K., Smith, S. L., Noetzli, J., Matthes, H., Vieira, G., Streletskiy, D. A., et al. (2019). Permafrost is warming at a global scale. *Nature Communications*, 10(1), 264. <https://doi.org/10.1038/s41467-018-08240-4>
- Boike, J., Nitzbon, J., Anders, K., Grigoriev, M., Bolshiyarov, D., Langer, M., et al. (2019). A 16-year record (2002–2017) of permafrost, active-layer, and meteorological conditions at the Samoylov Island Arctic permafrost research site, Lena River delta, northern Siberia: An opportunity to validate remote-sensing data and land surface, snow, and permafrost models. *Earth System Science Data*, 11(1), 261–299. <https://doi.org/10.5194/essd-11-261-2019>
- Carsel, R. F., & Parrish, R. S. (1988). Developing joint probability distributions of soil water retention characteristics. *Water Resources Research*, 24(5), 755–769. <https://doi.org/10.1029/WR024i005p00755>
- Cleary, E., Garbuno-Inigo, A., Lan, S., Schneider, T., & Stuart, A. M. (2021). Calibrate, emulate, sample. *Journal of Computational Physics*, 424, 109716. <https://doi.org/10.1016/j.jcp.2020.109716>
- Cuesta-Valero, F. J., Beltrami, H., Gruber, S., García-García, A., & González-Rouco, J. F. (2022). A new bootstrap technique to quantify uncertainty in estimates of ground surface temperature and ground heat flux histories from geothermal data. *Geoscientific Model Development*, 15(20), 7913–7932. <https://doi.org/10.5194/gmd-15-7913-2022>
- Dahl-Jensen, D., Mosegaard, K., Gundestrup, N., Clow, G. D., Johnsen, S. J., Hansen, A. W., & Balling, N. (1998). Past temperatures directly from the Greenland ice sheet. *Science*, 282(5387), 268–271. <https://doi.org/10.1126/science.282.5387.268>
- Dee, D. P., Uppala, S. M., Simmons, A. J., Berrisford, P., Poli, P., Kobayashi, S., et al. (2011). The ERA-Interim reanalysis: Configuration and performance of the data assimilation system. *Quarterly Journal of the Royal Meteorological Society*, 137(656), 553–597. <https://doi.org/10.1002/qj.828>
- Demezhko, D. Y., & Shchapov, V. A. (2001). 80,000 years ground surface temperature history inferred from the temperature–depth log measured in the superdeep hole SG-4 (the Urals, Russia). *Global and Planetary Change*, 29(3), 219–230. [https://doi.org/10.1016/S0921-8181\(01\)00091-1](https://doi.org/10.1016/S0921-8181(01)00091-1)
- Fritzsche, D., Schütt, R., Meyer, H., Miller, H., Wilhelms, F., Opel, T., & Savatugin, L. M. (2005). A 275 year ice-core record from akademii nauk ice cap, severnaya zemlya, Russian arctic. *Annals of Glaciology*, 42, 361–366. <https://doi.org/10.3189/172756405781812862>
- Garbuno-Inigo, A., Hoffmann, F., Li, W., & Stuart, A. M. (2020). Interacting langevin diffusions: Gradient structure and ensemble kalman sampler. *SIAM Journal on Applied Dynamical Systems*, 19(1), 412–441. <https://doi.org/10.1137/19M1251655>
- Gelman, A., Carlin, J. B., Stern, H. S., Dunson, D. B., Vehtari, A., & Rubin, D. B. (2013). *Bayesian data analysis* (3rd ed.). CRC Press. <https://doi.org/10.1201/b16018>
- Gilichinsky, D. A., Barry, R. G., Bykhovets, S. S., Sorokovikov, V. A., Zhang, T., Zudin, S. L., & Fedorov-Davydov, D. G. (1998). A century of temperature observations of soil climate: Methods of analysis and long-term trends. In A. Lewkowicz (Ed.), *Proceedings of the 7th international conference on permafrost* (Vol. 1, pp. 23–27). Univ. Laval, Yellowknife Northwest Territories.
- Groenke, B., Langer, M., & Miesner, F. (2024). Robust reconstruction of historical climate change from permafrost boreholes - data and code repository (v1.1) [Software]. <https://doi.org/10.5281/zenodo.11231742>
- Groenke, B., Langer, M., Nitzbon, J., Westermann, S., Gallego, G., & Boike, J. (2023). Investigating the thermal state of permafrost with Bayesian inverse modeling of heat transfer. *The Cryosphere*, 17(8), 3505–3533. <https://doi.org/10.5194/tc-17-3505-2023>
- Groenke, B., Nitzbon, J., & Langer, M. (2024). CryoGrid.jl: V0.21.0 [Software]. *Zenodo*. <https://doi.org/10.5281/zenodo.10659616>
- Guglielmin, M., Donatelli, M., Semplice, M., & Serra Capizzano, S. (2018). Ground surface temperature reconstruction for the last 500 years obtained from permafrost temperatures observed in the SHARE STELVIO Borehole, Italian Alps. *Climate of the Past*, 14(6), 709–724. <https://doi.org/10.5194/cp-14-709-2018>
- Harris, S. A., French, H. M., Heginbottom, J. A., Johnston, G. H., Ladanyi, B., Sego, D. C., & van Everdingen, R. O. (1988). *Glossary of permafrost and related ground-ice terms* (Technical Memorandum No. 142). National Research Council of Canada. Associate Committee on Geotechnical Research. Permafrost Subcommittee.
- Hartmann, A., & Rath, V. (2005). Uncertainties and shortcomings of ground surface temperature histories derived from inversion of temperature logs. *Journal of Geophysics and Engineering*, 2(4), 299–311. <https://doi.org/10.1088/1742-2132/2/4/S02>
- Hernández, A., Martín-Puertas, C., Moffa-Sánchez, P., Moreno-Chamarro, E., Ortega, P., Blockley, S., et al. (2020). Modes of climate variability: Synthesis and review of proxy-based reconstructions through the Holocene. *Earth-Science Reviews*, 209, 103286. <https://doi.org/10.1016/j.earscirev.2020.103286>
- Hopcroft, P. O., & Gallagher, K. (2023). Global variability in multi-century ground warming inferred from geothermal data. *Geophysical Research Letters*, 50(13), e2023GL104631. <https://doi.org/10.1029/2023GL104631>
- Hopcroft, P. O., Gallagher, K., & Pain, C. C. (2007). Inference of past climate from borehole temperature data using Bayesian reversible jump Markov chain Monte Carlo. *Geophysical Journal International*, 171(3), 1430–1439. <https://doi.org/10.1111/j.1365-246X.2007.03596.x>

- Huang, S., & Pollack, H. N. (1998). Global borehole temperature database for climate reconstruction. *IGBP PAGES/World Data Center-A for Paleoclimatology data contribution series*, 44.
- Huang, S., Pollack, H. N., & Shen, P.-Y. (2000). Temperature trends over the past five centuries reconstructed from borehole temperatures. *Nature*, 403(6771), 756–758. <https://doi.org/10.1038/35001556>
- Huang, S., Shen, P. Y., & Pollack, H. N. (1996). Deriving century-long trends of surface temperature change from borehole temperatures. *Geophysical Research Letters*, 23(3), 257–260. <https://doi.org/10.1029/96GL00020>
- Isaksen, K., Mühlh, D. V., Gubler, H., Kohl, T., & Sollid, J. L. (2000). Ground surface-temperature reconstruction based on data from a deep borehole in permafrost at Janssonhaugen, Svalbard. *Annals of Glaciology*, 31, 287–294. <https://doi.org/10.3189/172756400781820291>
- Isaksen, K., Nordli, Ø., Ivanov, B., Koltzow, M. A. Ø., Aaboe, S., Gjelten, H. M., et al. (2022). Exceptional warming over the Barents area. *Scientific Reports*, 12(1), 9371. <https://doi.org/10.1038/s41598-022-13568-5>
- Jaeger, J. C. (1965). Application of the theory of heat conduction to geothermal measurements. In *Terrestrial heat flow* (pp. 7–23). American Geophysical Union (AGU). <https://doi.org/10.1029/GM008p0007>
- Jahn, R., Blume, H. P., Asio, V. B., Spaargaren, O., & Schad, P. (2006). *Guidelines for soil description* (4th ed.). FAO.
- Jury, W. A., & Horton, R. (2004). *Soil physics*. John Wiley & Sons.
- Kneier, F., Overduin, P. P., Langer, M., Boike, J., & Grigoriev, M. N. (2018). Borehole temperature reconstructions reveal differences in past surface temperature trends for the permafrost in the Laptev Sea region. *Russian Arctic. Arktos*, 4(1), 1–17. <https://doi.org/10.1007/s41063-018-0041-3>
- Koopmans, R. W. R., & Miller, R. D. (1966). Soil freezing and soil water characteristic curves. *Soil Science Society of America Journal*, 30(6), 680–685. <https://doi.org/10.2136/sssaj1966.03615995003000060011x>
- Lachenbruch, A. H., & Marshall, B. V. (1986). Changing climate: Geothermal evidence from permafrost in the Alaskan Arctic. *Science*, 234(4777), 689–696. <https://doi.org/10.1126/science.234.4777.689>
- Langer, M., Nitzbon, J., Groenke, B., Assmann, L.-M., Schneider von Deimling, T., Stuenzi, S. M., & Westermann, S. (2024). The evolution of Arctic permafrost over the last 3 centuries from ensemble simulations with the CryoGridLite permafrost model. *The Cryosphere*, 18(1), 363–385. <https://doi.org/10.5194/tc-18-363-2024>
- Langer, M., Nitzbon, J., & Oehme, A. (2022a). CryoGridLite: Model input for Pan-Arctic simulations at 1° resolution from 1700 to 2020 [Dataset]. *Zenodo*. <https://doi.org/10.5281/zenodo.6619212>
- Langer, M., Nitzbon, J., & Oehme, A. (2022b). CryoGridLite: Model output of pan-Arctic simulations at 1° resolution from 1700 to 2020 [Dataset]. *Zenodo*. <https://doi.org/10.5281/zenodo.6619260>
- Langer, M., Westermann, S., Muster, S., Piel, K., & Boike, J. (2011). The surface energy balance of a polygonal tundra site in northern Siberia – Part 2: Winter. *The Cryosphere*, 5(2), 509–524. <https://doi.org/10.5194/tc-5-509-2011>
- Lunardini, V. (1978). Theory of n-factors and correlation of data. In *Proceedings of the third international conference on permafrost* (Vol. 1, pp. 40–46). National Research Council of Canada Ottawa.
- Mann, M. E., Rutherford, S., Bradley, R. S., Hughes, M. K., & Keimig, F. T. (2003). Optimal surface temperature reconstructions using terrestrial borehole data. *Journal of Geophysical Research*, 108(D7). <https://doi.org/10.1029/2002JD002532>
- Mann, M. E., & Schmidt, G. A. (2003). Ground vs. surface air temperature trends: Implications for borehole surface temperature reconstructions. *Geophysical Research Letters*, 30(12). <https://doi.org/10.1029/2003GL017170>
- Mareschal, J.-C., & Beltrami, H. (1992). Evidence for recent warming from perturbed geothermal gradients: Examples from Eastern Canada. *Climate Dynamics*, 6(3–4), 135–143. <https://doi.org/10.1007/BF00193525>
- Meyer, H., Opel, T., Laepple, T., Dereviagin, A. Y., Hoffmann, K., & Werner, M. (2015). Long-term winter warming trend in the Siberian Arctic during the mid-to late Holocene. *Nature Geoscience*, 8(2), 122–125. <https://doi.org/10.1038/ngeo2349>
- Mottaghy, D., & Rath, V. (2006). Latent heat effects in subsurface heat transport modelling and their impact on palaeotemperature reconstructions. *Geophysical Journal International*, 164(1), 236–245. <https://doi.org/10.1111/j.1365-246X.2005.02843.x>
- Nicolosky, D. J., & Romanovsky, V. E. (2018). Modeling long-term permafrost degradation. *Journal of Geophysical Research: Earth Surface*, 123(8), 1756–1771. <https://doi.org/10.1029/2018JF004655>
- Nitzbon, J., Krinner, G., Schneider Von Deimling, T., Werner, M., & Langer, M. (2023). First quantification of the permafrost heat sink in the Earth's climate system. *Geophysical Research Letters*, 50(12), e2022GL102053. <https://doi.org/10.1029/2022GL102053>
- NOAA National Centers of Environmental Information. (1999). Global surface summary of the day (v1.0) - station 21824099999 (Tiksi, RU) [Dataset]. <https://www.ncei.noaa.gov/access/metadata/landing-page/bin/iso?id=gov.noaa.ncdc:C00516:NCEIClimateDataOnline>
- Opel, T., Fritzsche, D., & Meyer, H. (2013). Eurasian Arctic climate over the past millennium as recorded in the Akademii Nauk ice core (Severnaya Zemlya). *Climate of the Past*, 9(5), 2379–2389. <https://doi.org/10.5194/cp-9-2379-2013>
- Painter, S. L., & Karra, S. (2014). Constitutive model for unfrozen water content in subfreezing unsaturated soils. *Vadose Zone Journal*, 13(4), 1–8. <https://doi.org/10.2136/vzj2013.04.0071>
- Park, H., Fedorov, A. N., Zheleznyak, M. N., Konstantinov, P. Y., & Walsh, J. E. (2015). Effect of snow cover on Pan-Arctic permafrost thermal regimes. *Climate Dynamics*, 44(9), 2873–2895. <https://doi.org/10.1007/s00382-014-2356-5>
- Phipps, S. J., McGregor, H. V., Gergis, J., Gallant, A. J., Neukom, R., Stevenson, S., et al. (2013). Paleoclimate data–model comparison and the role of climate forcings over the past 1500 years. *Journal of Climate*, 26(18), 6915–6936. <https://doi.org/10.1175/jcli-d-12-00108.1>
- Pollack, H. N., Demezhko, D. Y., Duchkov, A. D., Golovanova, I. V., Huang, S., Shchapov, V. A., & Smerdon, J. E. (2003). Surface temperature trends in Russia over the past five centuries reconstructed from borehole temperatures. *Journal of Geophysical Research*, 108(B4), 2002JB002154. <https://doi.org/10.1029/2002JB002154>
- Pollack, H. N., Huang, S., & Shen, P.-Y. (1998). Climate change record in subsurface temperatures: A global perspective. *Science (New York, N. Y.)*, 282(5387), 279–281. <https://doi.org/10.1126/science.282.5387.279>
- Rantanen, M., Karpechko, A. Y., Lippinen, A., Nordling, K., Hyvärinen, O., Ruosteenoja, K., et al. (2022). The Arctic has warmed nearly four times faster than the globe since 1979. *Communications Earth & Environment*, 3(1), 1–10. <https://doi.org/10.1038/s43247-022-00498-3>
- Ren, J., & Vanapalli, S. K. (2019). Comparison of soil-freezing and soil-water characteristic curves of two Canadian soils. *Vadose Zone Journal*, 18(1), 180185–180214. <https://doi.org/10.2136/vzj2018.10.0185>
- Riseborough, D. (1990). Soil latent heat as a filter of the climate signal in permafrost. In *Proceedings of the fifth Canadian permafrost conference, collection nordicana* (Vol. 54, pp. 199–205).
- Riseborough, D. W. (2002). The mean annual temperature at the top of permafrost, the TTOP model, and the effect of unfrozen water. *Permafrost and Periglacial Processes*, 13(2), 137–143. <https://doi.org/10.1002/ppp.418>
- Romanovsky, V. E., & Osterkamp, T. E. (2000). Effects of unfrozen water on heat and mass transport processes in the active layer and permafrost. *Permafrost and Periglacial Processes*, 11(3), 219–239. [https://doi.org/10.1002/1099-1530\(200007/09\)11:3\(219::AID-PPP352\)3.0.CO;2-7](https://doi.org/10.1002/1099-1530(200007/09)11:3(219::AID-PPP352)3.0.CO;2-7)

- Romanovsky, V. E., Sazonova, T. S., Balobaev, V. T., Shender, N. I., & Sergueev, D. O. (2007). Past and recent changes in air and permafrost temperatures in eastern Siberia. *Global and Planetary Change*, *56*(3), 399–413. <https://doi.org/10.1016/j.gloplacha.2006.07.022>
- Shen, P. Y., & Beck, A. E. (1991). Least squares inversion of borehole temperature measurements in functional space. *Journal of Geophysical Research*, *96*(B12), 19965–19979. <https://doi.org/10.1029/91JB01883>
- Shen, P. Y., Pollack, H. N., Huang, S., & Wang, K. (1995). Effects of subsurface heterogeneity on the inference of climate change from borehole temperature data: Model studies and field examples from Canada. *Journal of Geophysical Research*, *100*(B4), 6383–6396. <https://doi.org/10.1029/94JB03136>
- Swaminathan, C. R., & Voller, V. R. (1992). A general enthalpy method for modeling solidification processes. *Metallurgical Transactions A B*, *23*(5), 651–664. <https://doi.org/10.1007/BF02649725>
- van Genuchten, M. T. (1980). A closed-form equation for predicting the hydraulic conductivity of unsaturated soils. *Soil Science Society of America Journal*, *44*(5), 892–898. <https://doi.org/10.2136/sssaj1980.03615995004400050002x>
- Vasseur, G., Bernard, P., Van De Meulebrouck, J., Kast, Y., & Jolivet, J. (1983). Holocene paleotemperatures deduced from geothermal measurements. *Palaeogeography, Palaeoclimatology, Palaeoecology*, *43*(3–4), 237–259. [https://doi.org/10.1016/0031-0182\(83\)90013-5](https://doi.org/10.1016/0031-0182(83)90013-5)
- Wang, K. (1992). Estimation of ground surface temperatures from borehole temperature data. *Journal of Geophysical Research*, *97*(B2), 2095–2106. <https://doi.org/10.1029/91JB02716>
- Woodbury, A. D., & Ferguson, G. (2006). Ground surface paleotemperature reconstruction using information measures and empirical Bayes. *Geophysical Research Letters*, *33*(6). <https://doi.org/10.1029/2005GL025243>